J. Water Environ. Nanotechnol., 9(2): 196-210 Spring 2024

ORIGINAL RESEARCH PAPER

A Magnetic Nano adsorbent Based on Expanded Graphite with Enhanced Surface Area for the Removal of Sulfamethoxazole and Malachite Green from Aqueous Solutions

Asadollah Mohammadi*, Parisa Abedi, Mohammad Reza Gholami

Department of Applied Chemistry, Faculty of Chemistry, University of Guilan, Rasht, Iran

Received: 2023-12-13 Accepted: 2024-04-04 Published: 2024-05-12

ABSTRACT

In this study, a new magnetic nano adsorbent (denoted as Fe_3O_4/EXG/Cellulose) was synthesized using expanded graphite (EXG), microcrystalline cellulose, and Fe_3O_4 nanoparticles. The Fe_3O_4/EXG/Cellulose was used as an effective nano adsorbent for the removal of sulfamethoxazole (SMX) and malachite green (MG) from aqueous solutions using a batch process. The Fe_3O_4/EXG/Cellulose was fully characterized by the Fourier transform infrared (FT-IR), X-ray diffraction (XRD), Energy-dispersive X-ray spectroscopy (EDX), Brunauer-Emmett-Teller (BET), Field emission scanning electron microscopy (FESEM), and transmission electron microscopy (TEM) analyses. Based on the BET analysis, an improved surface area from 10.32 to 71.86 m^2 g^{-1} was achieved after the modification of expanded graphite using microcrystalline cellulose. The adsorption capacities for the MG dye and SMX drug were determined to be 109.9 and 3.9 mg/g, respectively. In addition, the adsorption process of SMX and MG by the Fe_3O_4/EXG/Cellulose was studied with isotherm and kinetic models. The results indicate the adsorption of SMX and MG by nanocomposite better described with pseudo-second-order kinetic. In addition, Langmuir and Freundlich isotherm models well describe the adsorption of MG and SMX using Fe_3O_4/EXG/Cellulose, respectively. Furthermore, Fe_3O_4/EXG/Cellulose can be easily recycled and reused over 5 times and keeps a high level of adsorption efficiency.

Keywords: *Nanoadsorbent; Expanded graphite; Microcrystalline cellulose; Sulfamethoxazole; Malachite green.*

How to cite this article

Mohammadi A., Abedi P., Gholami M. R., A Magnetic Nano adsorbent Based on Expanded Graphite with Enhanced Surface Area for the Removal of Sulfamethoxazole and Malachite Green from Aqueous Solutions. J. Water Environ. Nanotechnol., 2024; 9(2): 196-210. DOI: 10.22090/jwent.2024.02.06

INTRODUCTION

Removal of organic pollutants has acquired increasing attention in recent years due to their high toxicity and stability in the environment. Pharmaceuticals and industrial dyes as indicative pollutants of this group enter the environment largely because of their important roles in many applications, such as human medical practices, agriculture, personal care, paper, plastics, cosmetics, and textiles. These industries discharge untreated wastes into the water bodies, which creates serious problems and various diseases for the environment and human health [1-5]. Among the antibiotics, sulfamethoxazole (SMX), as a top-selling sulfonamide antibiotic, has been intensively investigated by many researchers because of its vital roles in many bacterial infections such as urinary tract infections, bronchitis, and prostatitis. SMX is also used to prevent and treat a certain type of pneumonia [6-8]. On the other hand, organic dyes are extensively used in many industries, such as textiles, paper, coatings, and leather. However, most of the organic dyes are toxic and their discharge to

* Corresponding Authors Email: *a_mohammadi@guilan.ac.ir*

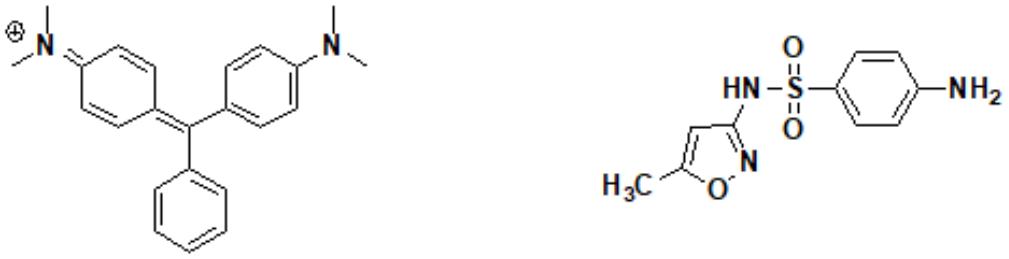

Scheme 1. Selected chemical properties of pollutants

the environment causes serious problems to human health and other living organisms. Malachite green (MG) as a toxic dye is frequently used as an antifungal agent in aquaculture and many chemical industries [9-12]. Therefore, materials with high absorption efficiency can be considered to remove these contaminants. Among the carbon materials, expanded graphite (EG), with excellent stability, low density, production on a large scale, large specific surface area, and having many oxygen-based functional groups on the surface can improve adsorption efficiency. In addition, EG with unique properties has been intensively studied by many researchers from different fields [13-18]. On the other hand, EG has a small particle size and can be dispersed and float on the surface of the water after purification processes. Therefore, these restrictions limit its use in high-volume aquatic environments. Surface modification of EG with suitable modifiers like cellulose can improve its surface area and absorbance properties for water purification. Furthermore, the addition of magnetic nanoparticles to EG can simplify its application for adsorption processes [19-21]. Therefore, cellulose and graphite-based materials are preferred for adsorption applications due to their availability in large quantities, easy separation and recycling from solution, and relatively low price. Unfortunately, the production of such adsorbent at low cost and industrial scale and impacts on human life and the environment remains challenging. In addition, there are still technical challenges in the use of nano adsorbents in water purification.

Here, Fe_3O_4/EXG/Cellulose was synthesized from low-cost cellulose and graphite-based material and used for the efficient removal of the SMX drug and MG dye from water. The morphology and structure of Fe_3O_4/EXG/Cellulose were carefully analyzed, and its adsorption capacity was discussed in detail for SMX and MG. The adsorption kinetic and adsorption isotherms were subsequently studied. In addition, Fe_3O4/EXG/Cellulose can be easily recycled and reused over 5 times and keeps a high level of adsorption efficiency.

MATERIALS AND METHODS

Materials

Natural Flake (expandable) graphite (particle size < 80 mesh), Microcrystalline cellulose, malachite green hydrochloride, sulfamethoxazole, Iron (III) chloride hexahydrate, Iron (II) sulfate heptahydrate and ammonium hydroxide were supplied by Sigma-Aldrich and used as received. Table S1 (supporting information) displays the chemical name, CAS registry number, source, and purity (%) of materials used. In addition, the chemical structures of adsorbates are presented in Scheme 1. To preparation of aqueous solutions, deionized water was used throughout the experiment. The stock solutions were prepared by dissolving a certain amount of MG and SMX. The mixtures for adsorption processes were centrifuged on a Hettich Universal II, Germany at 200 rpm for 10 min. The absorption spectra of solutions were recorded on a UNICO UV2150 Spectrophotometer in the range of 200-800 nm. FT-IR spectra of samples in KBr pellets were recorded on a Shimadzu 8400 FT-IR spectrophotometer. TEM and FESEM images

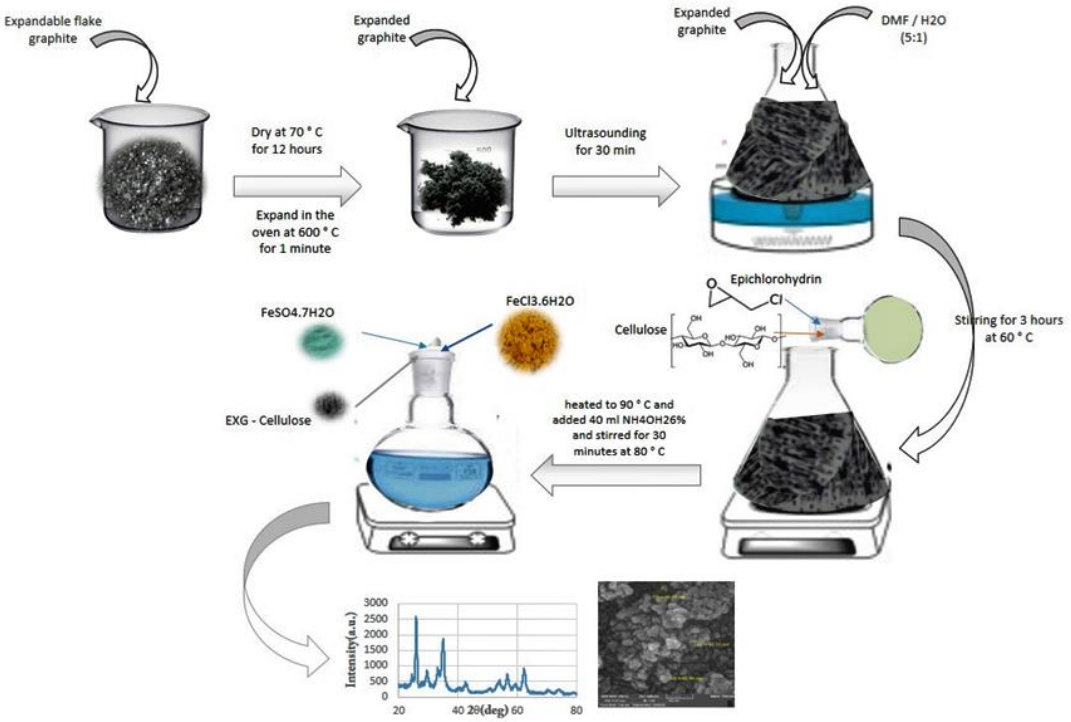

Fig. 1. The preparation process of the nano adsorbent Fe_3O_4/EXG/Cellulose

of expanded graphite (EXG), EXG-Cellulose, and Fe_3O_4/EXG-Cellulose were obtained by a transmission electron microscope (Philips CM120, Netherlands) and field emission scanning electron microscopy (TESCAN MIRA III). The XRD graphs of samples were achieved using a Phillips PW 1730. The specific surface area of expanded graphite (EXG) and Fe_3O_4/EXG/Cellulose were analyzed by the nitrogen gas adsorption method using a BET apparatus (Belsorp mini II, Bel Japan Inc., Japan).

Preparation of Fe_3O_4/EXG/Cellulose nanocomposite

Fe_3O_4/EXG/Cellulose nanocomposite was fabricated in three steps as follows. In the first step of the nanocomposite preparation process, the expandable graphite powder was dried at 70 °C in a drying oven for 12 h to minimize absorbed moisture. The expandable graphite was then developed into expanded graphite via high-temperature expansion at 700 °C for 60 s [16]. The resulting expanded graphite (EXG) was then cooled naturally in a desiccator. Then, to improve the surface of EX, 1.0 g of EXG at DMF/H_2O (400 mL, 5:1, v/v) was first sonicated for 30 min at 40 °C and then mixed with epoxidized cellulose. Epoxidation of microcrystalline cellulose was carried out using epichlorohydrin (EP) in the presence of sodium hydroxide according to the previous procedure reported [9, 22]. After reaction completion, the solution pH was adjusted to 7.0 using an aqueous solution of H_2SO_4 (0.5 M). The achieved EXG-Cellulose was washed with distilled water several times and then dried at 70 °C in a drying oven for 24 h. Finally, nanocomposite magnetic expanded graphite/cellulose (Fe_3O_4/EXG/Cellulose) was prepared by hydrothermal method and the details were as follows: In detail, 6.0 g of $FeCl_3 \bullet 6H_2O$ and 4.0 g of $FeSO_4 \bullet 7H_2O$ were blended in 100 mL of deionized water and the achieved solution was then heated to 90 °C. The resulting solution pH was adjusted to 10.0 by the addition of 40 mL of ammonia solution (solution A). Finally, 1.0 g of EXG-Cellulose was dispersed in 20 mL of ethanol sonicated for 20 min and then added into solution A. The resulting solution was continuously stirred in refluxing condition for 30 min. The mixture was cooled and the magnetic EXG-Cellulose was separated by an external magnet, washed fully with distilled water and ethanol, and then dried at 60 ˚C for 12 h. The preparation process of the nano adsorbent Fe_3O_4/EXG-Cellulose is schematically shown in Fig. 1.

Table 1. Adsorption equilibrium isotherm equations and adsorption kinetic models

Model	Equation	Reference
Langmuir	$\frac{1}{q_e}=\frac{1}{K_L Q_m C_e}+\frac{1}{Q_m}$	[9, 11]
Separation factor	$R_L=\frac{1}{1+C_0 K_L}$	
Freundlich	$\log q_e=\log K_F+\frac{1}{n}\log C_e$	[9, 11]
Pseudo-first-order kinetic model	$\ln(q_e-q_t)=\ln q_e-k_1 t$	[9, 23]
Pseudo-second-order kinetic model	$\frac{t}{q_t}=\frac{1}{k_2 q_e^2}+\frac{t}{q_e}$	[9, 23]

Nomenclature: q_m (mg/g): Langmuir maximum biosorption capacity, K_L (L/mg): Langmuir constant, C_0 (mg/L): highest initial concentration; K_F ((mg/g) (L/mg)$^{1/n}$): Freundlich constant, n: Freundlich exponent; b_T (J/mol): pseudo-first-order rate constant; k_2 (g/(mg min)): pseudo-second-order rate constant; β (g/mg).

Adsorption experiments

The batch adsorption study was used to evaluate the Fe_3O_4/EXG/Cellulose performance for adsorption of MG and SMX from aqueous solutions. Experiments were conducted by adding a quantitative amount of Fe_3O_4/EXG/Cellulose into 10 mL of solution containing MG or SMX and then adjusting the initial pH with a dilute solution of NaOH or HCl. The adsorption experiment was continued in a shaking bath with 200 rpm at 25 °C. The nano adsorbent Fe_3O_4/EXG/Cellulose was then separated by an external magnet. The residual concentration of MG and SMX in solutions was evaluated by UV–Vis spectrophotometer. The wavelengths of maximum absorption for MG or SMX were 621 nm and 259 nm, respectively. The adsorption capacity (q; mgg^{-1}) of Fe_3O_4/EXG/Cellulose and dye removal efficiency (R%) at the equilibrium and time t was calculated from the equations 1 and 2:

$$q_e=\frac{(C_0-C_e)V}{m} \quad \text{(Eq. 1)}$$

$$R\ (\%)=\frac{100\ (C_0-C_e)}{C_0} \quad \text{(Eq. 2)}$$

Where C_0 (mg/L) and C_e (mg/L), are MG and SMX concentrations at the initial and equilibrium, respectively, m is the weight of Fe_3O_4/EXG/Cellulose (g) and V is the volume of the solution (L).

In addition, two adsorption kinetic models including pseudo-first order and pseudo-second order kinetic models were used to evaluate MG and SMX adsorption by Fe_3O_4/EXG/Cellulose. Two adsorption isotherms including Langmuir, and Freundlich models were also used to assess for MG and SMX adsorption by fabricated Fe_3O_4/EXG/Cellulose. Adsorption kinetics and isotherm equations used in this study are listed in Table 1.

RESULTS AND DISCUSSION

Morphology and chemical structure characterization

The XRD, FTIR, FESEM, EDS, TEM, and BET analyses were used for chemical structural determination and morphologies of fabricated

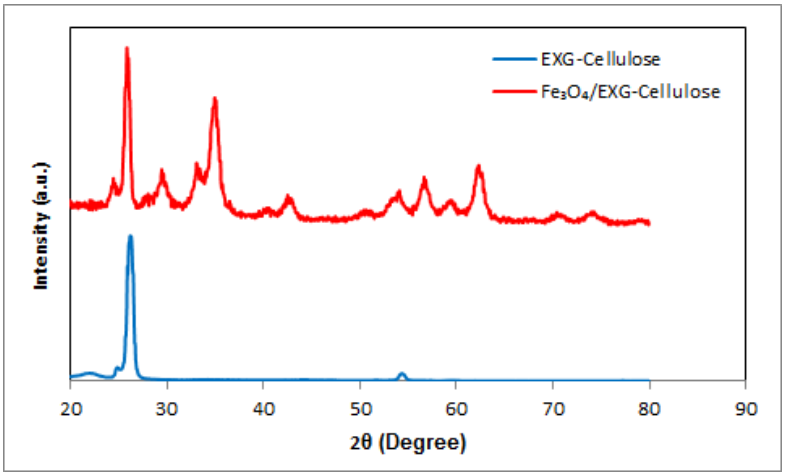

Fig. 2. The XRD patterns of cellulose-functionalized expanded graphite (EXG/Cellulose) and fabricated magnetite nanocomposite (Fe_3O_4/EXG/Cellulose).

graphite-based nanocomposites. Fig. 2 shows the XRD patterns of cellulose-functionalized expanded graphite (EXG/Cellulose) and synthesized magnetite nanocomposite (Fe_3O_4/EXG/Cellulose). As shown in Fig. 2, the crystal structure of expanded graphite (2θ = 26.1°, 52.4°) was not changed after chemical modification with microcrystalline cellulose. A characteristic and broad peak at 2θ = 20.2° in the XRD pattern of EXG-Cellulose was observed, which is attributed to the microcrystalline cellulose. As revealed by the XRD pattern of the Fe_3O_4/EXG/Cellulose, in Fig. 2, all diffraction peaks of the Fe_3O_4/EXG-Cellulose fit well with those of Fe_3O_4, cellulose, and expanded graphite. Therefore, the characteristic peaks of Fe_3O_4 nanoparticles were observed at 2θ = 29.2, 32.9, 34.7, 41.9, 53.7, 57.2, 62.1, 69.8 and 72.3° (JCPDS card no.: 75-0449).

For characterization of the functional groups on nanocomposites, the FT-IR spectra of EXG, EXG/Cellulose, and Fe_3O_4/EXG/Cellulose were prepared (Fig. 3). The strong peaks at 3451 cm^{-1} and 2927 cm^{-1} in the FT-IR patterns of EXG, EXG/Cellulose, and Fe_3O_4/EXG/Cellulose, are assigned to the stretching vibration of O-H and aliphatic C-H groups, respectively. As shown in Fig. 3, the peak corresponding to the C-O group in EXG/Cellulose is observed at 1070 cm^{-1} after the modification of expanded graphite with microcrystalline cellulose. Moreover, the newly emerged vibrational peaks at 579 and 634 cm^{-1} in the FT-IR spectra of Fe_3O_4/EXG/Cellulose are assigned to the stretching vibration of the Fe-O group originating from Fe_3O_4 NPs (Fig. 3). The observation of functional peaks after the modification and magnetization, suggests that the structure of EXG and Cellulose is not destroyed during the reaction. In addition, the FTIR spectra of Fe_3O_4/EXG/Cellulose before and after adsorption of MG and SMX were displayed in Fig. S1 (supporting information). From the FTIR analysis, it is clear that the MG and SMX were adsorbed effectively by Fe_3O_4/EXG/Cellulose.

The FESEM images of EXG and Fe_3O_4/EXG/Cellulose are presented in Fig. 4. As shown in Fig. 4a, the plates, layers, and wormlike graphite rods were formed from the expandable graphite after being placed in the oven at 700 °C. After chemical modification of EXG with microcrystalline cellulose using epichlorohydrin as a crosslinker, layers and a lot of pores in the FESEM images of EXG/Cellulose were observed (Fig. 4b). In the final magnetite nanocomposite (Fe_3O_4/EXG/Cellulose), the number of cavities and specific surface area has increased, as confirmed by the FESEM images (Figure 4c-d) and BET analysis (Fig. 6), respectively. The adsorption ability of nanocomposite Fe_3O_4/EXG/Cellulose toward pollutants improves with an increase in the specific surface area and pores. In addition, the elemental microanalysis (wt %) of fabricated nanocomposites including EXG, EXG/Cellulose, and Fe_3O_4/EXG/Cellulose was illustrated in Table 2. From the EDX results, the elements with weight percentages C (88.24) and O (11.76) were detected in expanded graphite. For effective

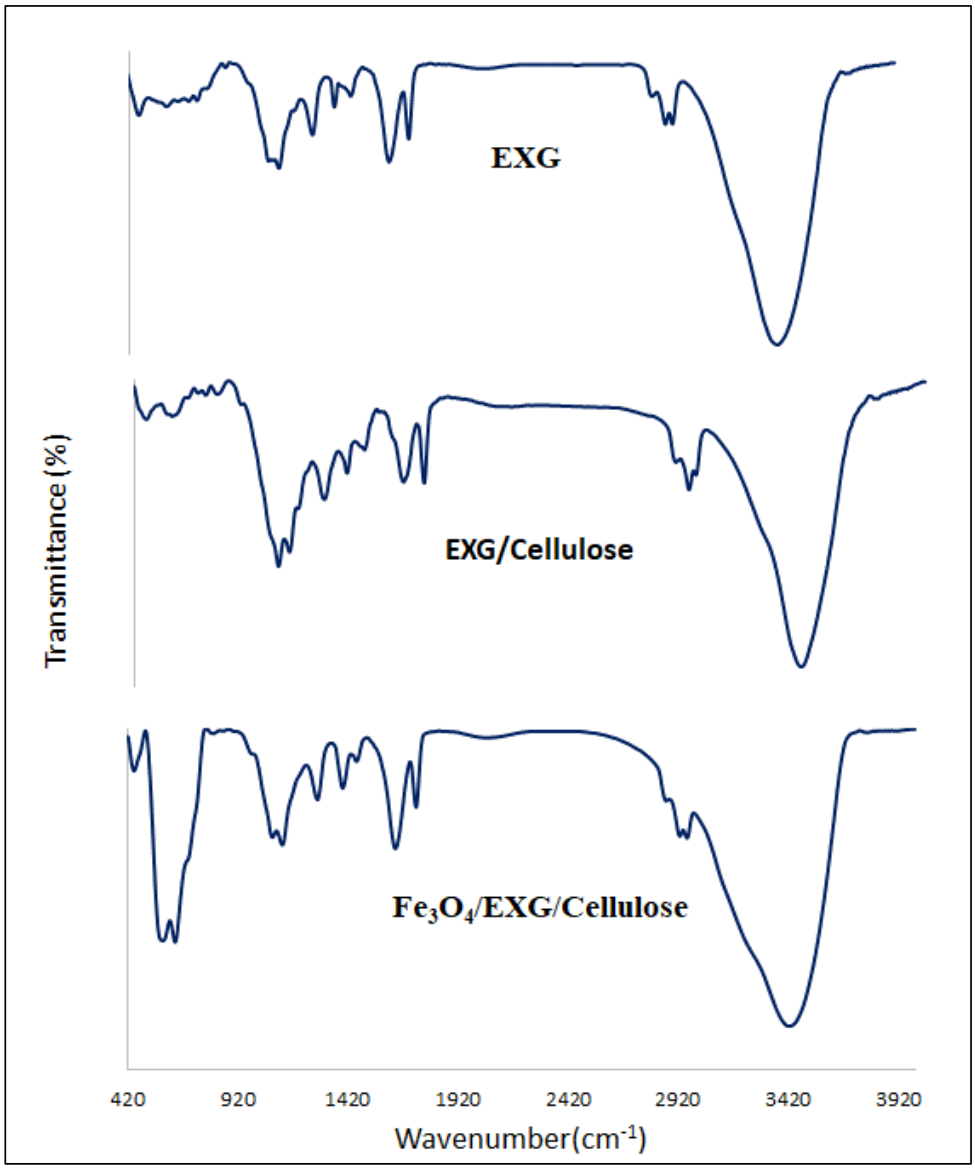

Fig. 3. The FTIR spectra of EXG, EXG/Cellulose and Fe_3O_4/EXG/Cellulose.

Table 2. The elemental microanalysis (wt %) of EXG, EXG/Cellulose and Fe_3O_4/EXG/Cellulose

Sample	Element weight percentage			
	Fe	O	C	N
EXG	-	11.76	88.24	-
EXG/Cellulose	-	26.04	73.96	-
Fe_3O_4/EXG/Cellulose	80.38	4.31	14.75	0.57

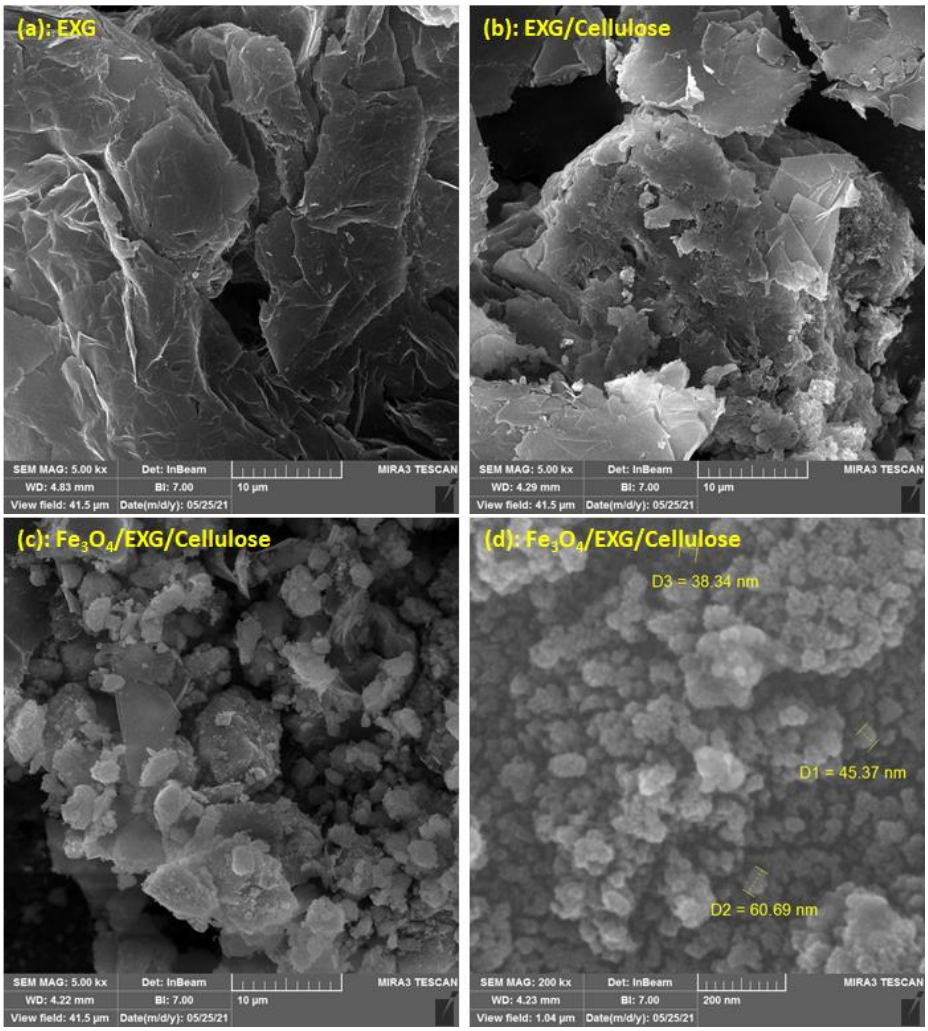

Fig. 4. FESEM images of EXG (a), EXG/Cellulose (b), and Fe_3O_4/EXG/Cellulose (c &d) nanocomposites.

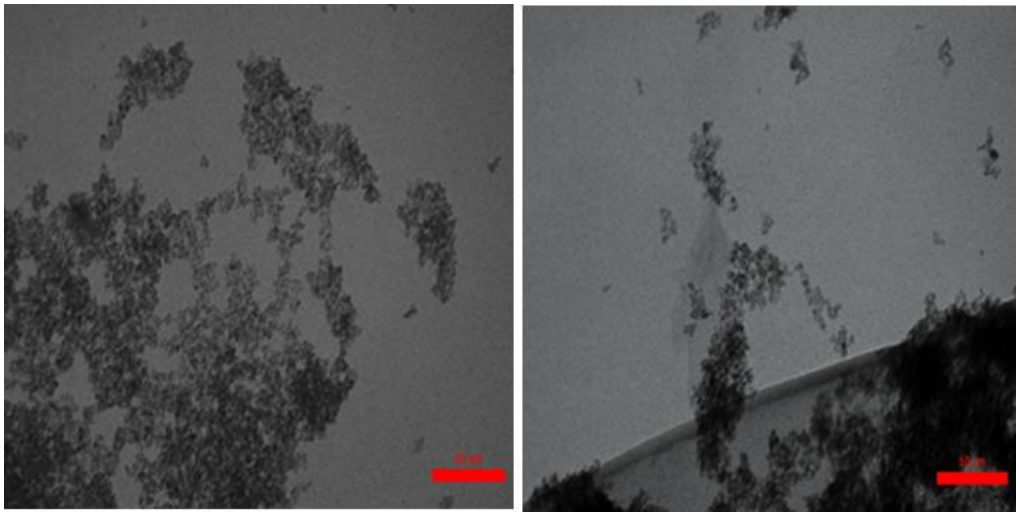

Fig. 5. TEM images of Fe_3O_4/EXG/Cellulose nanocomposite.

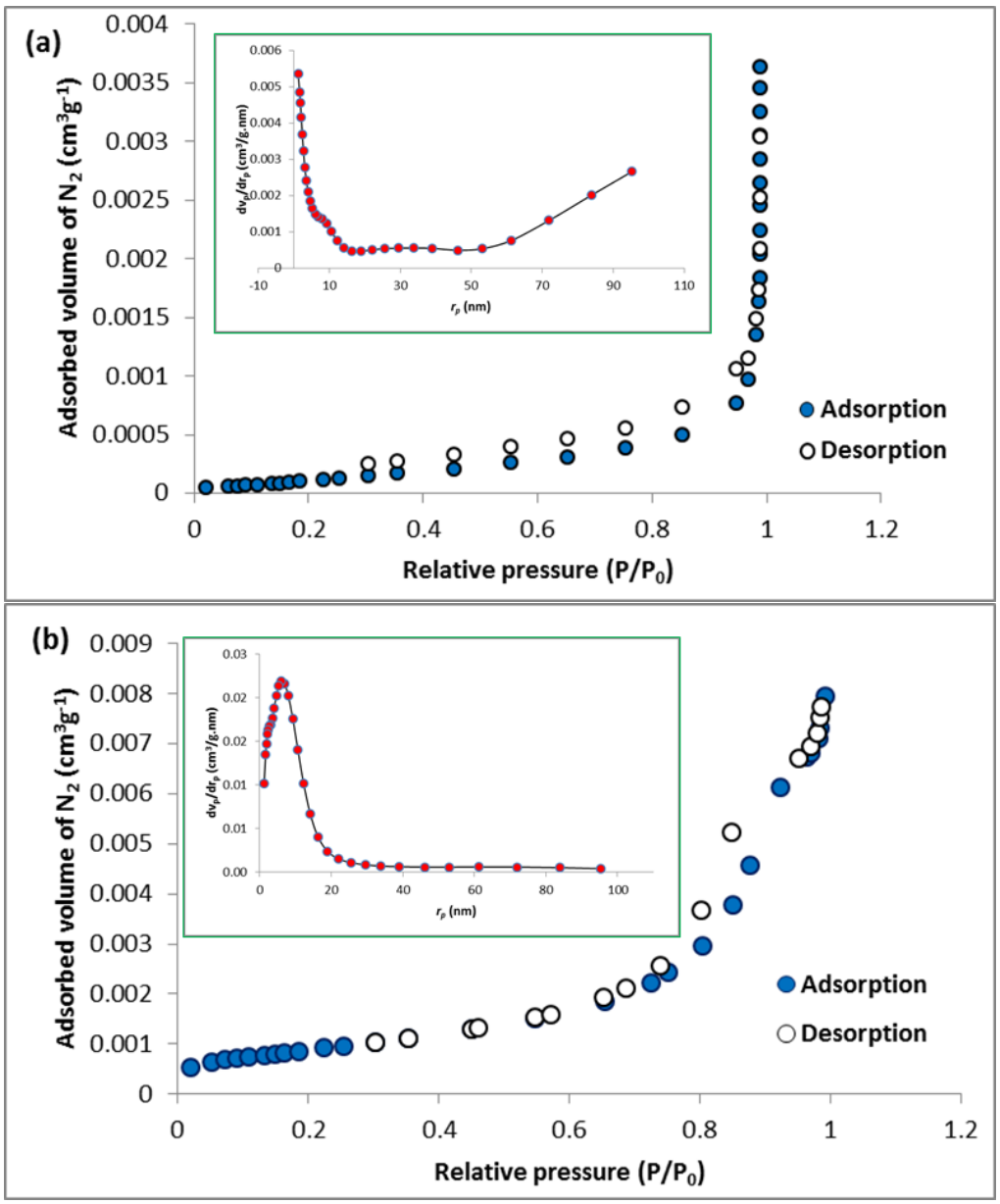

Fig. 6. (a) Nitrogen adsorption-desorption isotherms of EXG (the insert is the corresponding pore size distribution curve); (b) Nitrogen adsorption-desorption isotherms of Fe_3O_4/EXG/Cellulose (the insert is the corresponding pore size distribution curve).

interaction of EXG with microcrystalline cellulose, the oxygen content has increased in nanocomposite EXG/Cellulose by approximately 15 weight %. Furthermore, compared with EXG/Cellulose, the elemental microanalysis of Fe_3O_4/EXG/Cellulose confirmed the presence of iron, suggesting that the EXG/Cellulose were successfully magnetized by Fe_3O_4 NPs.

Additionally, TEM images of Fe_3O_4/EXG/Cellulose display uniformly sized particles with nano-dimensions and little aggregation (Fig. 5).

Fig. 6 shows the BET isotherms of EXG and Fe_3O_4/EXG/Cellulose and corresponding pore size distribution curves. Based on the BET analysis, the specific surface area ($a_{s,BET}$) of EXG and Fe_3O_4/EXG/Cellulose was obtained as 10.13 and 71.86 $m^2\ g^{-1}$, respectively (Table 3). Thus, an improved surface area was achieved after the chemical modification of

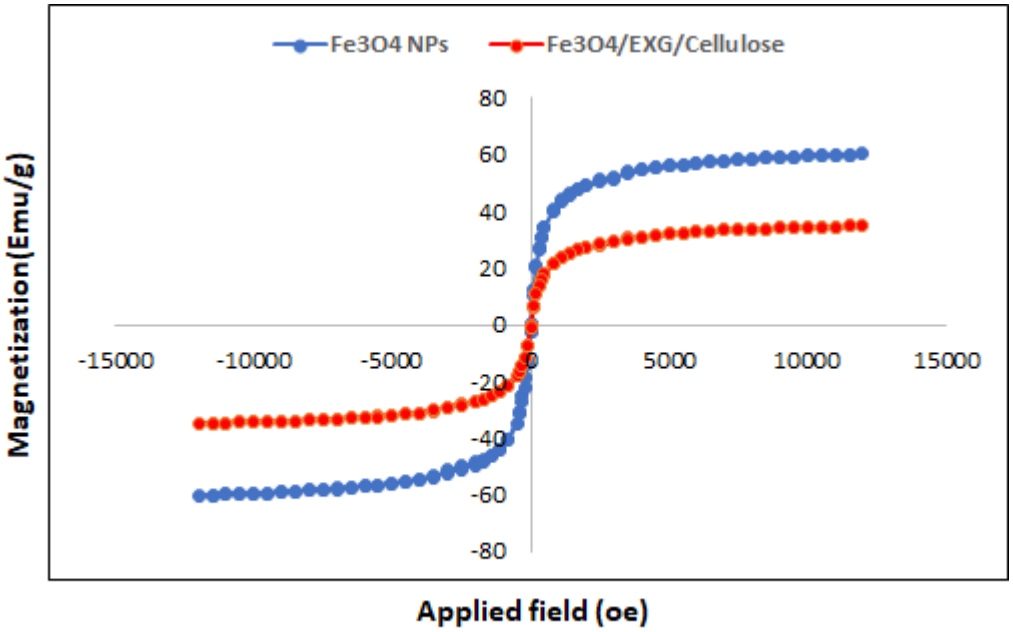

Fig. 7. Magnetization curves of the Fe_3O_4 NPs and Fe_3O_4/EXG/Cellulose at room temperature.

Table 3. The surface area, pore size, and total pore volume of EXG, and Fe_3O_4/EXG/Cellulose

Sample	Surface area ($m^2 g^{-1}$)	Mean pore diameter (nm)	Total pore volume ($cm^3 g^{-1}$)
EXG	10.13	47.6	0.120
Fe_3O_4/EXG/Cellulose	71.86	15.1	0.271

expanded graphite with microcrystalline cellulose. In addition, corresponding pore size distribution curves EXG and Fe_3O_4/EXG-Cellulose with average sizes of 47.6 nm and 15.1 nm are observable in Fig. 6, which are suitable for the removal of various organic pollutants.

In addition, the magnetic behavior of the Fe_3O_4 NPs and Fe_3O_4/EXG/Cellulose was studied by VSM analysis. Fig. 7 revealed that the saturation magnetization values of Fe_3O_4 NPs and Fe_3O_4/EXG/Cellulose were 60.2 and 34.8 emu/g, respectively. Fe_3O_4/EXG/Cellulose displayed a lower magnetization saturation value compared with pure Fe_3O_4 NPs, suggesting that the surface of Fe_3O_4 NPs was effectively coated by the nonmagnetic expanded graphite and microcrystalline cellulose. However, the Fe_3O_4/EXG/Cellulose was easily separated from the aqueous solution by the application of an external magnetic field.

Adsorption performance

pH effect on the adsorption of SMX and MG

The pH point of zero charge (pHpzc) of Fe_3O_4/EXG/Cellulose was performed over the pH range from 3.0 to 12.0, and the result is displayed in Fig. S2 (supporting information). According to the pH changes of the solution, the pHpzc of the nanocomposite Fe_3O_4/EXG/Cellulose is found to be pH = 6.38. This result shows that the surface of Fe_3O_4/EXG/Cellulose is positively charged in pH values below the pH = 6.38, and at pH values higher than the pH_{PZC}, the Fe_3O_4/EXG/Cellulose surface is negatively charged. Therefore, the aqueous solutions of pollutants were adjusted to

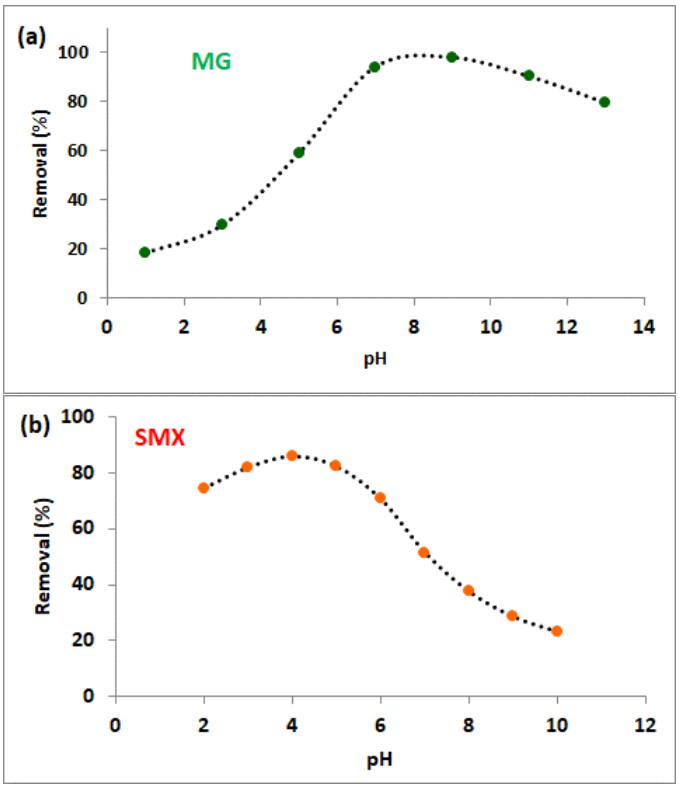

Fig. 8. pH effect on the adsorption of SMX and MG by Fe_3O_4/EXG/Cellulose.

Table 4. The pseudo-first-order and pseudo-second-order kinetic fitting parameters for the adsorption of MG and SMX on the Fe_3O_4/EXG/Cellulose

	Pseudo-first-order				Pseudo-second-order			
Pollutant	Q_e(mg/g)	Q_{cal}(mg/g)	K_1(1/min)	R^2	Q_e(mg/g)	Q_{cal}(mg/g)	K_2(g/(mg*min)	R^2
MG	79.1	80.34	0.064	0.96	79.1	88.49	0.001	0.99
SMX	2.53	1.948	0.023	0.67	2.53	3.36	0.006	0.98

pH ranging from 1 to 13 for MG and 2 to 10 for SMX by 1.0 M HCl and 1.0 M NaOH. The initial concentrations were set to 200 mg/L for MG and 20 mg/L for SMX. For the adsorption tests, 0.025 and 0.05 mg Fe_3O_4/EXG/Cellulose were employed each time for the adsorption of MG and SMX, respectively, where the adsorption was conducted at 25 °C for durations until the equilibrium of adsorption. Several functional groups like -OH and $-NH_2$ groups have existed in Fe_3O_4/EXG/Cellulose, and they can interact effectively with different pollutants. Meanwhile, most pollutants are charged when the pH values of the solutions are changed. The adsorption behaviors of Fe_3O_4/EXG/Cellulose for MG and SMX were evaluated under different pH values (Fig. 8). As shown in Fig. 8a, the removal performance of Fe_3O_4/EXG/Cellulose for the cationic MG dye was gradually enhanced with the increase of the pH values. Upon increasing the pH values higher than 7, the surface of the adsorbent

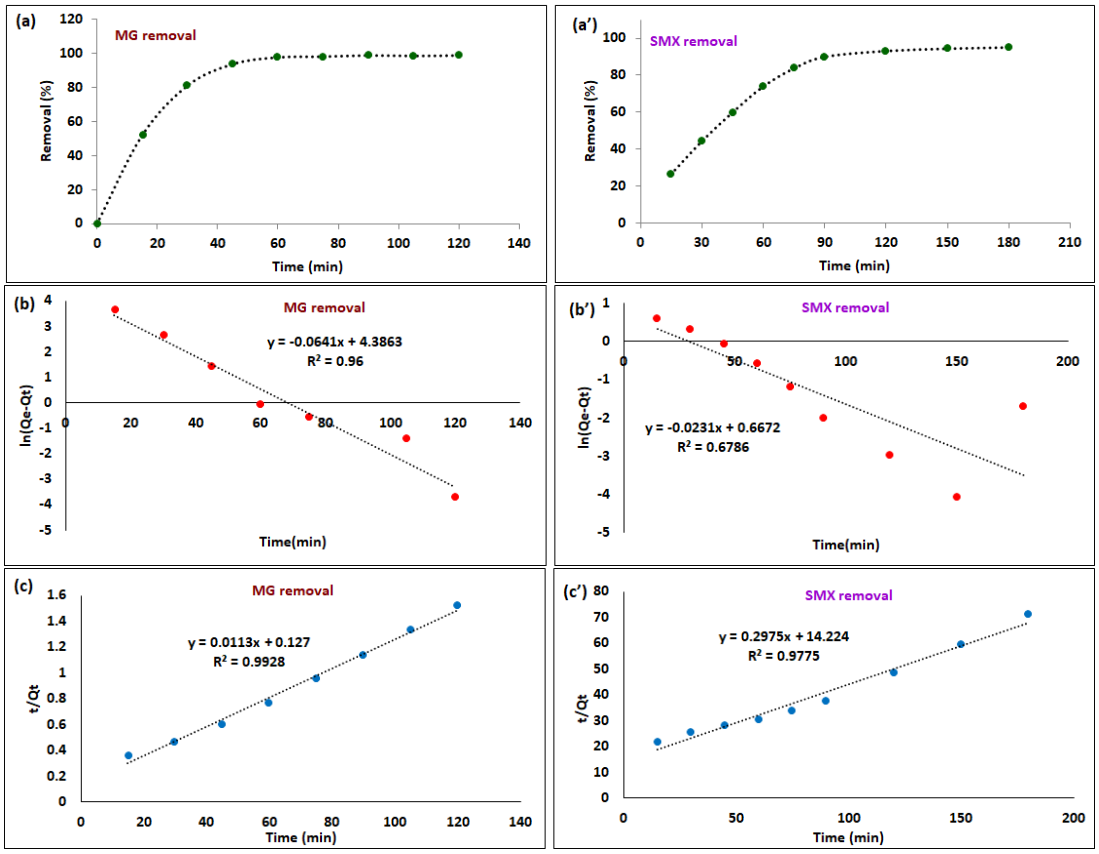

Fig. 9. The effect of contact time on the adsorption of the MG and SMX on the Fe_3O_4/EXG/Cellulose (a-a'), Pseudo-first-order fitting curves for the adsorption of MG and SMX (b-b'), and the corresponding pseudo-second-order fitting curves for the adsorption of MG and SMX on the Fe_3O_4/EXG/Cellulose (c-c').

is easily deprotonated (pHpzc = 6.38), thus the removal efficiencies for the cationic MG dye were remarkably enhanced. The higher adsorption performance of fabricated adsorbent resulted from the hydrogen bonding and the electrostatic attraction between the negatively charged adsorbent and the cationic MG dye. However, the adsorption efficiencies of sulfamethoxazole (SMX) were high in acidic conditions, especially when pH = 4 (Fig. 8b). This is the result of the strong hydrogen bonding and electrostatic attraction between the protonated adsorbent and the negatively charged SMX. Remarkably, nearly 90 % of the SMX was removed from the water with a pH value of 4.

Adsorption kinetic study

Fig. 9 shows the adsorption kinetic study of the fabricated adsorbent (Fe_3O_4/EXG/Cellulose) for the removal of the MG dye and SMX drug. As shown in Figs. 9a-a', the equilibrium status can be reached within 45 min and 90 min for MG dye and SMX drug, respectively, suggesting the rapid adsorption of these pollutants by Fe_3O_4/EXG/Cellulose. This is an excellent property of our fabricated adsorbent to allow the fast treatment of pollutants in the industry. To describe the adsorption processes of the MG and SMX by Fe_3O_4/EXG/Cellulose, the two kinetic models including pseudo-first-order and pseudo-second-order kinetic models were applied (Table 1, Figs. 9b-c'). Furthermore, the fitting parameters thus obtained are listed in Table 4. The higher R^2 values obtained from the pseudo-second-order kinetic model suggest that the adsorption of MG and SMX on Fe_3O_4/EXG/Cellulose was mainly described by the chemical adsorption [9, 11, 24]. However, the R^2 and Q_{cal} values obtained from the pseudo-first-order are also reasonable to describe

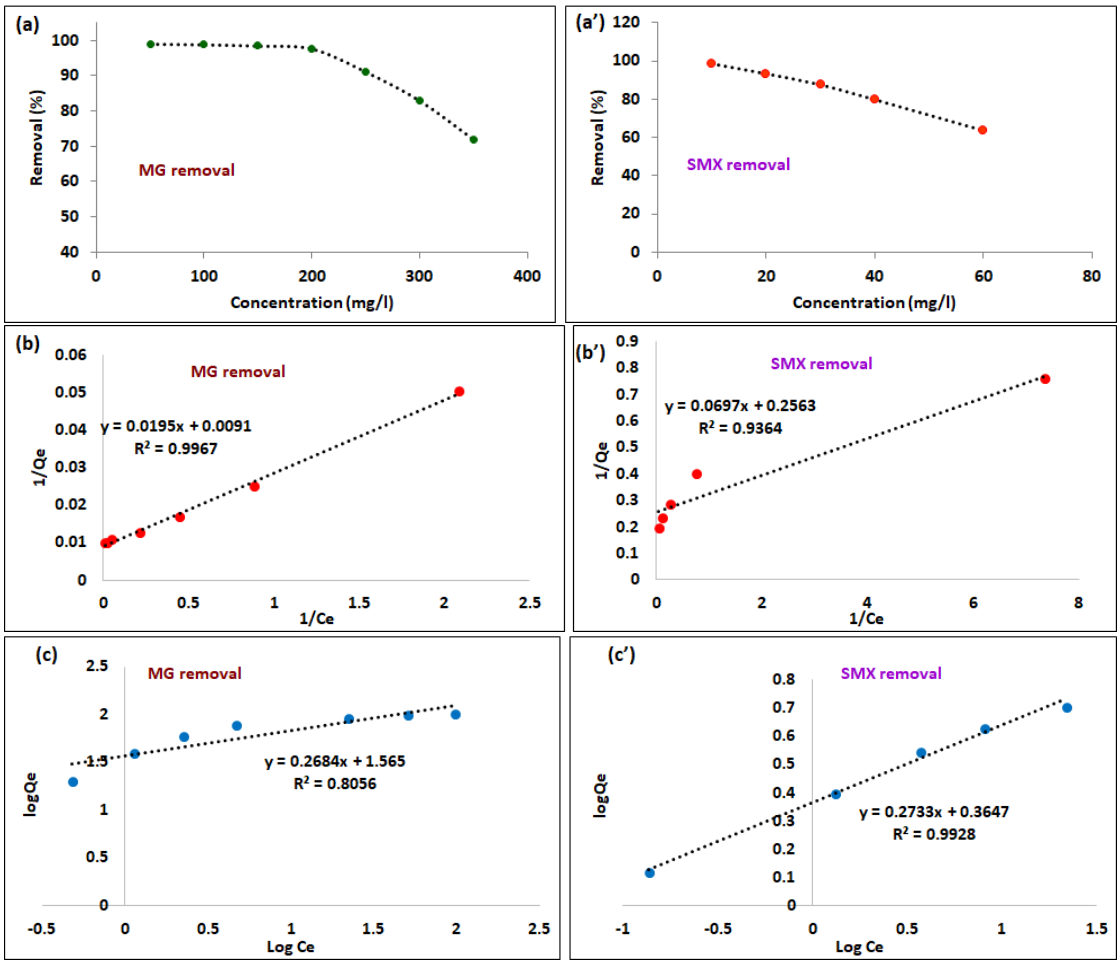

Fig. 10. The effect of initial concentration of Mg and SMX on the adsorption behavior of the Fe_3O_4/EXG/Cellulose (a-a'), The adsorption isotherms of MG and SMX on Fe_3O_4/EXG/Cellulose according to Langmuir equation (b-b') and Freundlich equation (c-c').

the adsorption behavior of MG by Fe_3O_4/EXG/Cellulose.

Adsorption isotherms of Fe_3O_4/EXG/Cellulose

The two adsorption isotherm models, including Langmuir and Freundlich models (Table 1) were selected to study the interaction mechanism of the adsorbent Fe_3O_4/EXG/Cellulose and the pollutants MG and SMX (Fig. 10). The Langmuir isotherm model applies to monolayer molecular adsorption on the homogeneous adsorbent surface, while the Freundlich isotherm model is applied to multilayer molecular adsorption with inhomogeneous active sites on the adsorbent surface, where the stronger binding sites are occupied preferentially and the other sites are filled up subsequently [25]. According to the results in Fig. 10 and Table 5, the maximum adsorption capacities of Fe_3O_4/EXG/Cellulose toward MG and SMX were 109.9 and 3.9 mg/g, respectively. Furthermore, the correlation coefficients R^2 of the Langmuir equation for MG and SMX were 0.996 and 0.936, respectively. However, the R^2 values obtained by the Freundlich equation for MG and SMX were 0.805 and 0.992, respectively. These results proposed that the adsorption of MG dye by the Fe_3O_4/EXG/Cellulose was consistent with the Langmuir equation, while the adsorption of SMX drug by the Fe_3O_4/EXG/Cellulose predominantly proceeds through the Freundlich isotherm model.

Adsorption thermodynamics

The effect of different temperature ranges (283-353 K) for the adsorption of MG and

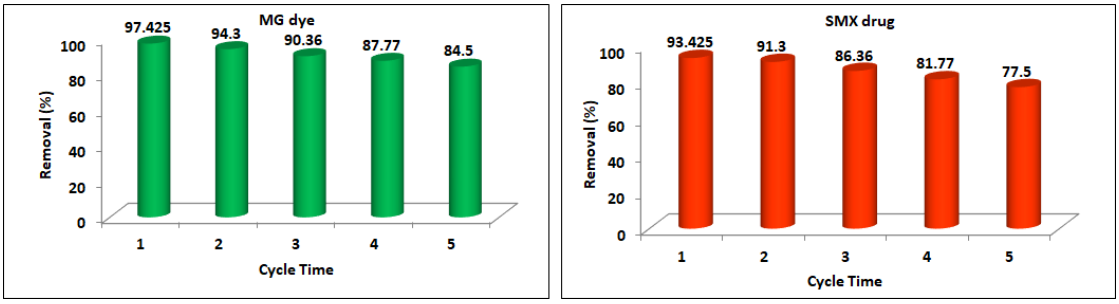

Fig. 11. The removal efficiency of MG (a) and SMX (b) by Fe_3O_4/EXG/Cellulose after five adsorption-desorption cycles.

Table 5. Summary of experimental data and adsorption isotherm fitting parameters for the adsorption of MG and SMX on Fe_3O_4/EXG/Cellulose

Pollutant	Langmuir model			Freundlich model		
	Q_m(mg/g)	K_L(L/mg)	R^2	1/n	K_F(L/mg)	R^2
MG	109.89	0.466	0.996	0.2684	36.72	0.805
SMX	3.9	3.678	0.936	0.2733	2.315	0.992

SMX on Fe_3O_4/EXG/Cellulose was studied and thermodynamic parameters were determined using equations 3-4. As shown in Figure S3, and Table S2 (supporting information), ΔH° is greater than 0 for MG adsorption, which suggests that heating favors the adsorption of MG on Fe_3O_4/EXG/Cellulose. In addition, the negative value of ΔG° indicates that the adsorption of MG dye by Fe_3O_4/EXG/Cellulose is a spontaneous process. On the other hand, both calculated thermodynamic parameters ΔH° and ΔG° for adsorption of SMX drug on Fe_3O_4/EXG/Cellulose are negative, indicating that the exothermic and spontaneous adsorption process.

$$\Delta G^\circ = -RT \ln K_c \quad \text{(Eq. 3)}$$

Desorption and recycle studies

The fabricated adsorbents for application in related industries must be stable, inexpensive, and reusable. In this experiment, to evaluate the regeneration ability of Fe_3O_4/EXG/Cellulose, the five adsorption-desorption cycles for MG and SMX were performed using water-ethanol as eluent (Fig. 11). As shown in Fig. 11, there are negligible changes in the removal efficiencies of MG and SMX by Fe_3O_4/EXG/Cellulose after 5 cycles. However, even after 5 adsorption-desorption cycles, the adsorption capacity of Fe_3O_4/EXG/Cellulose remains high, so the removal rates of MG dye and SMX drug were still maintained as more than 84% and 77%, respectively. These findings indicate that Fe_3O_4/EXG/Cellulose can be easily regenerated in synthetic wastewater treatment and keeps a high level of adsorption efficiency.

CONCLUSION

Here, a new magnetic nano adsorbent based on expanded graphite and microcrystalline cellulose (Fe_3O_4/EXG/Cellulose) with high water stability was fabricated. Based on the BET analysis, an improved surface area from 10.32 to 71.86 $m^2\ g^{-1}$ was achieved after the modification and magnetization of expanded graphite using microcrystalline cellulose. The Fe_3O_4/EXG/Cellulose with a large specific surface area and abundant active sites showed a high adsorption capacity for the removal of MG dye and SMX drug. The results also indicate the adsorption of

SMX and MG by nanocomposite better described with pseudo-second-order kinetic. In addition, Langmuir and Freundlich isotherm models well describe the adsorption of MG and SMX using Fe_3O_4/EXG/Cellulose, respectively. The maximum adsorption capacities of Fe_3O_4/EXG/Cellulose toward MG and SMX were 109.9 and 3.9 mg/g, respectively. Moreover, Fe_3O_4/EXG/Cellulose exhibited good recyclability, so the removal rates of MG dye and SMX drug were still maintained at more than 84% and 77%, respectively. These results showed that Fe_3O_4/EXG/Cellulose is a nano adsorbent with high dye and drug adsorption capacities that are capable of use in wastewater remediation.

CONFLICTS OF INTEREST

Ethics approval: This research did not contain any studies involving animal or human participants. No specific permission was required for this work.

Consent to participate: Not applicable.

Consent for publication: Not applicable.

Authors Contributions:

All authors contributed to the study's conception and design. Investigation, material preparation, data collection, and analysis were performed by Parisa Abedi and Mohammad Reza Gholami. The first draft of the manuscript was written by Parisa Abedi and Asadollah Mohammadi. Asadollah Mohammadi also reviewed and approved the final manuscript.

Funding: Not applicable.

Competing interests: The authors declare no competing interests.

Acknowledgments

The authors thank the Research Council of the University of Guilan for the financial support of this research work.

ABBREVIATIONS

EXG, expanded graphite; SMX, sulfamethoxazole; MG, malachite green; NPs, nanoparticles; FT-IR, Fourier transform infrared; XRD, X-ray diffraction; EDX, Energy-dispersive X-ray spectroscopy; BET, Brunauer-Emmett-Teller; FESEM, Field emission scanning electron microscopy; TEM, transmission electron microscopy (TEM).

REFERENCES

[1] Z. Liu, T.A. Khan, M.A. Islam and U. Tabrez, Bioresour. Technol. 354,127168 (2022). https://doi.org/10.1016/j.biortech.2022.127168

[2] S. Bakhshi Nejad and A. Mohammadi, J. Chem. Eng. Data 65, 2731 (2020). https://doi.org/10.1021/acs.jced.0c00063

[3] M. Bilal, I. Ihsanullah, M.U.H. Shah, A.V.B. Reddy and T.M. Aminabhavi, J. Environ. Manage. 321, 115981 (2022). https://doi.org/10.1016/j.jenvman.2022.115981

[4] G. Prasannamedha and P.S. Kumar, J. Clean. Prod. 250, 119553 (2020). https://doi.org/10.1016/j.jclepro.2019.119553

[5] E. Omrani, A. Ahmadpour, M. Heravi, and T.R. Bastami, J. Water Process. Eng. 47, 102581 (2022). https://doi.org/10.1016/j.jwpe.2022.102581

[6] P.S. Delghandi, V. Soleimani, B.S. Fazly Bazzaz and H. Hosseinzadeh, Naunyn Schmiedebergs Arch. Pharmacol. 396, 2667 (2023). https://doi.org/10.1007/s00210-023-02490-w

[7] Y.Y. Deng, M.Y. Zou, W. Liu, Y.L. Lian, Q.M. Guo, X.M. Zhang and A. Dan, A. J. Clean. Prod. 394, 136271 (2023). https://doi.org/10.1016/j.jclepro.2023.136271

[8] P. Sarker, X. Lei, K. Taylor, W. Holmes, H. Yan, D. Cao, M.E. Zappi and D.D. Gang, Chem. Eng. J. 454, 140082 (2023). https://doi.org/10.1016/j.cej.2022.140082

[9] A. Mohammadi and P. Veisi, J. Environ. Chem. Eng. 6, 4634 (2018). https://doi.org/10.1016/j.jece.2018.07.002

[10] M.F. Siddiqui, S.A. Khan, D. Hussain, U. Tabrez, I. Ahamad, T. Fatma, T.A. Khan, Ind. Crops Prod. 176, 114301 (2022). https://doi.org/10.1016/j.indcrop.2021.114301

[11] S.H. Mousavi, F. Shokoofehpoor and A. Mohammadi, J. Chem. Eng. Data 64, 135 (2018). https://doi.org/10.1021/acs.jced.8b00656

[12] B.S. Rathi, P.S. Kumar, and D.V.N. Vo, Sci. Total Environ. 797, 149134 (2021). https://doi.org/10.1016/j.scitotenv.2021.149134

[13] A. Celzard, J.F. Mareche and Furdin, Carbon 40, 2713 (2002). https://doi.org/10.1016/S0008-6223(02)00183-5

[14] Y. Tian, H. Ma and B. Xing, Appl. Surf. Sci. 537, 147995 (2021). https://doi.org/10.1016/j.apsusc.2020.147995

[15] R. Bentini, A. Pola, L.G. Rizzi, A. Athanassiou and D. Fragouli, Chem. Eng. J. 372, 1174 (2019). https://doi.org/10.1016/j.cej.2019.04.196

[16] G. Fang, M. Yu, K. Meng, F. Shang and X. Tan, Energy & Fuels 34, 10109 (2020). https://doi.org/10.1021/acs.energyfuels.0c00955

[17] Y. Liu, B. Sun, J. Li, D. Cheng, X. An, B. Yang, Z. He, R. Lutes, A. Khan and Y. Ni, ACS Sustain. Chem. Eng. 6, 3291 (2018). https://doi.org/10.1021/acssuschemeng.7b03456

[18] M. Cuccarese, S. Brutti, A. De Bonis, R. Teghil, I. Mancini, S. Masi and D. Caniani, Sci. Rep. 11, 3427 (2021). https://doi.org/10.1038/s41598-021-83117-z

[19] V. Mahmoodi, T.R. Bastami, and A. Ahmadpour, Environ. Sci. Pollut. Res. 25, 8268 (2018). https://doi.org/10.1007/s11356-018-1224-y

[20] Y. Tian, H. Ma and B. Xing, Appl. Surf. Sci. 537, 147995 (2021).

https://doi.org/10.1016/j.apsusc.2020.147995
[21] K.H. Wu, W.C. Huang, W.C. Hung and Tsai, Mater. Sci. Eng. B 266, 115068 (2021). https://doi.org/10.1016/j.mseb.2021.115068
[22] K. Ma, Y. Liu, Z. Xie, R. Li, Z. Jiang, X. Ren and T.S. Huang, Ind. Eng. Chem. Res. 52, 7413 (2013). https://doi.org/10.1021/ie400122h
[23] S.M. Mousavi and A. Mohammadi, Process Saf. Environ. Prot. 114, 1 (2018). https://doi.org/10.1016/j.psep.2017.12.004
[24] E. Martwong, S. Chuetor and J. Junthip, Polym. 14, 342 (2022). https://doi.org/10.3390/polym14112199
[25] X. Feng, B. Qiu and D. Sun, Sep. Purif. Technol. 290, 120837 (2022). https://doi.org/10.1016/j.seppur.2022.120837